Check for updates

ASME Journal of Electronic Packaging
Online journal at:
https://asmedigitalcollection.asme.org/electronicpackaging

Kaiying Jiang
Department of Mechanical Engineering,
Stanford University,
Stanford, CA 94305

Daeyoung Kong
Department of Mechanical Engineering,
Stanford University,
Stanford, CA 94305

Sreekant Narumanchi
National Renewable Energy Laboratory,
Golden, CO 80401

James W. Palko
Department of Mechanical Engineering,
University of California, Merced,
Merced, CA 95343

Ercan M. Dede
Electronics Research Department,
Toyota Research Institute of North America,
Ann Arbor, MI 48105

Chulmin Ahn
Advanced Drive Concept Development,
Hyundai Motor Company,
Gyeonggi-do 18280, South Korea

Hyoungsoon Lee
Mechanical Engineering Department,
Chung-Ang University,
Seoul 06974, South Korea

Mehdi Asheghi
Department of Mechanical Engineering,
Stanford University,
Stanford, CA 94305

Kenneth E. Goodson
Department of Mechanical Engineering,
Stanford University,
Stanford, CA 94305

Mitigation of Boiling-Induced Thermal Degradation Using Microporous Nickel Inverse Opals Structures

Engineered microporous structures have received much attention in high-heat-flux electronics cooling due to their high thermal conductivity and permeability, and large surface area for heat transfer, but are susceptible to boiling-induced thermal degradation. This study investigates the efficacy of nickel inverse opals (NiIOs) in mitigating structural degradation caused by corrosion-assisted erosion during pool boiling with water as the working fluid. First, we compared the reliability of NiIOs to copper inverse opals (CuIOs) for a 3-day pool boiling test at constant heat flux. The NiIOs demonstrated superior resistance to thermal degradation due to their inherent corrosion resistance and mechanical strength. Subsequently, we conducted a more controlled experiment to show the effect of heat flux on the degradation of the NiIOs while excluding the effect of temperature variations. Pool boiling tests of 20-μm-thickness NiIOs covering an area of $\sim 11 \times 11\,mm^2$ with a $2.5 \times 2.5\,mm^2$ heater at the center were conducted at heat flux levels of 20%, 40%, and 60% of the critical heat flux (CHF) for 3 days. The NiIOs subjected to heat flux levels of 20% and 40% CHF showed minimal degradation, while the sample subjected to 60% CHF showed erosion on the top surface due to higher bubble formation and departure rate. These results show the potential of NiIOs as a promising solution for long-term thermal management in high-power electronic devices, although design considerations for maximum allowable heat flux are necessary for reliable operation.
[DOI: 10.1115/1.4069315]

Keywords: boiling-induced degradation, nickel inverse opal, copper inverse opal, erosion, corrosion, thermal degradation

1 Introduction

The enhancement of boiling heat transfer is critical in thermal management systems for high-power electronic devices, where efficient heat removal is essential to maintain operational integrity and prevent failure [1,2]. In recent years, microporous materials have emerged as promising candidates for enhancing heat transfer due to their unique structural properties [3,4]. Among these porous materials, copper inverse opals (CuIOs) have gained attention for their exceptional thermal conductivity and tunable permeability [5,6]. However, CuIOs' susceptibility to structural degradation over time during boiling poses significant reliability concerns [7,8]. Degradation of CuIOs' pore and neck structures caused by corrosion-assisted erosion was observed in as little as 3 days under pool boiling conditions in water [7]. This deterioration affects the thermal performance and long-term efficacy of CuIOs.

In this paper, we explore the potential of nickel inverse opals (NiIOs) in mitigating boiling-induced thermal degradation. NiIOs

The International Technical Conference on Packaging and Integration of Electronic and Photonic Microsystems (InterPACK) Hotel FERA Anaheim, a DoubleTree by Hilton. InterPACK2024.

Contributed by the Electronic and Photonic Packaging Division of ASME for publication in the Journal of Electronic Packaging. Manuscript received January 11, 2025; final manuscript received March 19, 2025; published online September 10, 2025. Assoc. Editor: Cheng Chen.

This work is in part a work of the U.S. Government. ASME disclaims all interest in the U.S. Government's contributions.

 Copyright © 2025 by ASME

Downloaded from http://asmedigitalcollection.asme.org/electronicpackaging/article-pdf/147/4/041107/7524913/ep-25-1004.pdf by Stanford University user on 15 September 2025

offer a promising solution to these reliability challenges with their inherent corrosion resistance and mechanical strength [9,10]. Here, we first compare the pool boiling performance of NiIOs and CuIOs over 3 days, where 10-μm-thick IO structures covering an area of $11 \times 11\,mm^2$ were heated uniformly with a $10 \times 10\,mm^2$ serpentine heater, supplying a constant heat flux at 115 W cm^{-2}. The topology and elemental composition of the surface after the 3-day pool boiling test were analyzed using scanning electron microscopy (SEM) and X-ray photoelectron spectroscopy (XPS). In the second half of this study, a more controlled test was conducted to study the effect of heat flux and bubble dynamics on NiIOs' reliability. NiIOs of 20-μm-thickness covering $11 \times 11\,mm^2$ area were heated by a $2.5 \times 2.5\,mm^2$ mesh heater at various heat fluxes. The temperature history and topology of IO structures after boiling are discussed. This study offers valuable insights into strategies for mitigating long-term pool-boiling-induced structural degradation, paving the pathway for high-heat-flux thermal management solutions that are both high-performing and reliable.

2 Methodology

2.1 Fabrication of Nickel Inverse Opals. Figure 1 details the fabrication process of NiIOs. A seed layer of 20-nm Ti and 100-nm Au was first evaporated onto a 550-μm-thick silicon (Si) wafer. Polystyrene spherical beads (ThermoFisher, Invitrogen, Waltham, MA) of diameter 4.8 μm, in 5% weight/volume solution, were dispensed onto the seed layer. The sample was then left at ambient conditions for water to evaporate and form a random-packed template [5]. Then, to create interconnected necks between spheres to enhance permeability, the beads were sintered at 100 °C for 80 min. Neck–pore ratio d_n/d_p can be tuned by adjusting the sintering temperature and time [5]. During electroplating, the sample was placed in 1 M $NiSO_4 + 0.2$ M $NiCl_2 + 0.6$ M H_3BO_3 solution, facing a Ni plate as a counter electrode. The thickness of NiIOs was controlled by changing the electroplating time and current density, j. To fabricate 20-μm-thick NiIOs on the Au seed layer, electroplating process was continued for 1.5 h at $j = 5$ mA cm^{-2}. After the electrodeposition, the polystyrene beads were dissolved by immersing the sample in tetrahydrofuran for at least 24 h. The sample was then immersed in de-ionized (DI) water, ethanol, isopropyl alcohol, and acetone for cleaning.

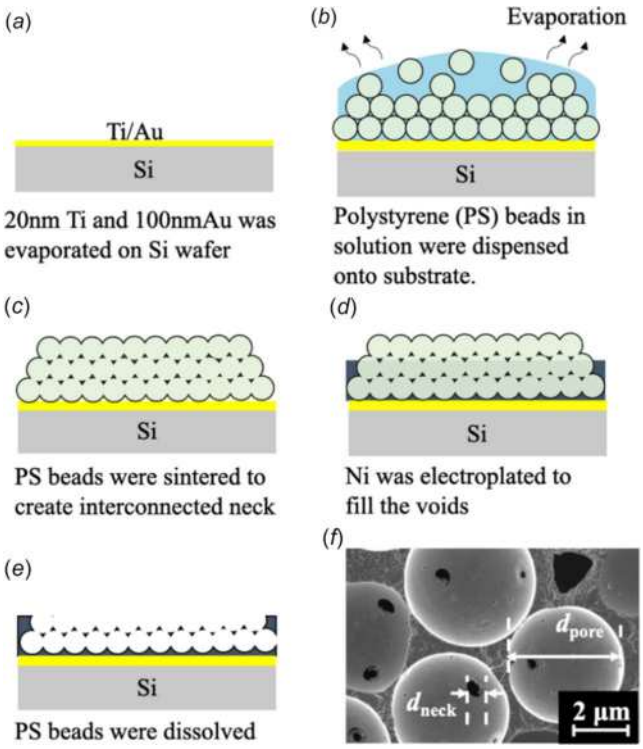

Fig. 1 (*a*)–(*e*) Fabrication process of NiIOs and (*f*) top view SEM of NiIOs of pore diameter 4.8 μm. Neck-to-pore ratio is estimated to be 0.14. Figure adapted from Ref. [8].

2.2 Procedure of Pool Boiling Tests. The pool boiling apparatus shown in Fig. 2 consists of a $150 \times 150 \times 150\,mm^3$ chamber (Ideal Vacuum, Albuquerque, NM) with aluminum alloy as a frame. Side walls with various port openings were assembled to allow access to thermocouples, cartridge heater, condenser coil, and sample holder. Type-T thermocouples (OMEGA, Stamford, CT) were used to measure liquid and vapor temperature. Two cartridge heaters (Heating Element Plus, 250 W, Nashville, TN) were inserted to heat working fluid DI water to saturation temperature. The condenser coil was connected to a water-based external chiller (Thermo Electron RTE-7, Waltham, MA) operating at 85 °C. To remove any noncondensable gas, DI was boiled rigorously using cartridge heaters for over 30 min before each test. The chamber was at atmospheric pressure throughout the test.

To supply uniform heat flux to the inverse opals, a resistive heater was patterned on the backside of the silicon. Metal layers of 20 nm titanium and 70 nm platinum were evaporatively coated onto the surface, resulting in a final resistance of around 30 Ω. Two types of heater designs were used in this study: serpentine and mesh. However, the heater design variation did not significantly affect the IO performance, as concluded from previous experimental and simulation work [7,8]. The current and voltage pads were connected to a DC power supply and data acquisition (NI 9220, Austin, TX) for power supply and monitor. The heated region was coated with black paint of $\varepsilon = 0.94$ for the infrared (IR) camera (FLIR A655, Boston, MA) reading. The sample was then fixed onto a three-dimensional-printed sample holder with silicone epoxy.

In Secs. 3.1 and 3.2, the reported base IO temperature, T_{base}, was calculated by subtracting temperature drop in the silicon substrate from IR-captured average heater temperature, $T_{heater,avg}$, assuming one-dimensional conduction in silicon

$$T_{base} = T_{heater,avg} - q'' \frac{t_{Si}}{k_{Si}} \tag{1}$$

where q'' is the supplied heat flux, t_{Si} is the silicon substrate thickness, and k_{Si} is the conductivity of silicon at the temperature $T_{heater,avg}$.

3 Results and Discussion

Two subsections are included in the results and discussion. First, a comparison between CuIOs and NiIOs pool boiling reliability performance is made to investigate NiIOs' potential in mitigating thermal degradation. The second section focuses on a more controlled NiIOs reliability test, discussing the effect of heat flux and bubble dynamics while maintaining the same NiIOs temperature.

3.1 Nickel Inverse Opals Potential in Mitigating Degradation. Figure 3(*a*) shows the pool boiling curve of CuIOs and NiIOs, conducted at 1.01×10^5 Pa with DI water as the working fluid. Both the CuIOs and NiIOs samples were of thickness 8 μm (i.e., ~1.5 to 2 layers), neck-to-pore ratio 0.14, covering $11 \times 11\,mm^2$. The patterned resistive heater covered a $10 \times 10\,mm^2$ region. The critical heat fluxes (CHFs) were 190 W cm^{-2} at a superheat of 15.4 °C, and 180 W cm^{-2} at a superheat of 13.1 °C, for CuIOs and NiIOs, respectively.

The reliability test was conducted at a heat flux well below CHF for safety. For both CuIOs and NiIOs, the heat flux was maintained throughout 3 days at 115 W cm^{-2}, supplied by the $10 \times 10\,mm^2$ heater. It should be noted that the neck-to-pore ratio and thickness of samples used in the reliability and CHF tests are slightly different. Smaller neck-to-pore ratio leads to smaller permeability [5]. Thicker IO structures can cause difficulty for the vapor to escape, decreasing the CHF value [11]. Despite these differences, the temperature

Downloaded from http://asmedigitalcollection.asme.org/electronicpackaging/article-pdf/147/4/041107/7524913/ep-25-1004.pdf by Stanford University user on 15 September 2025

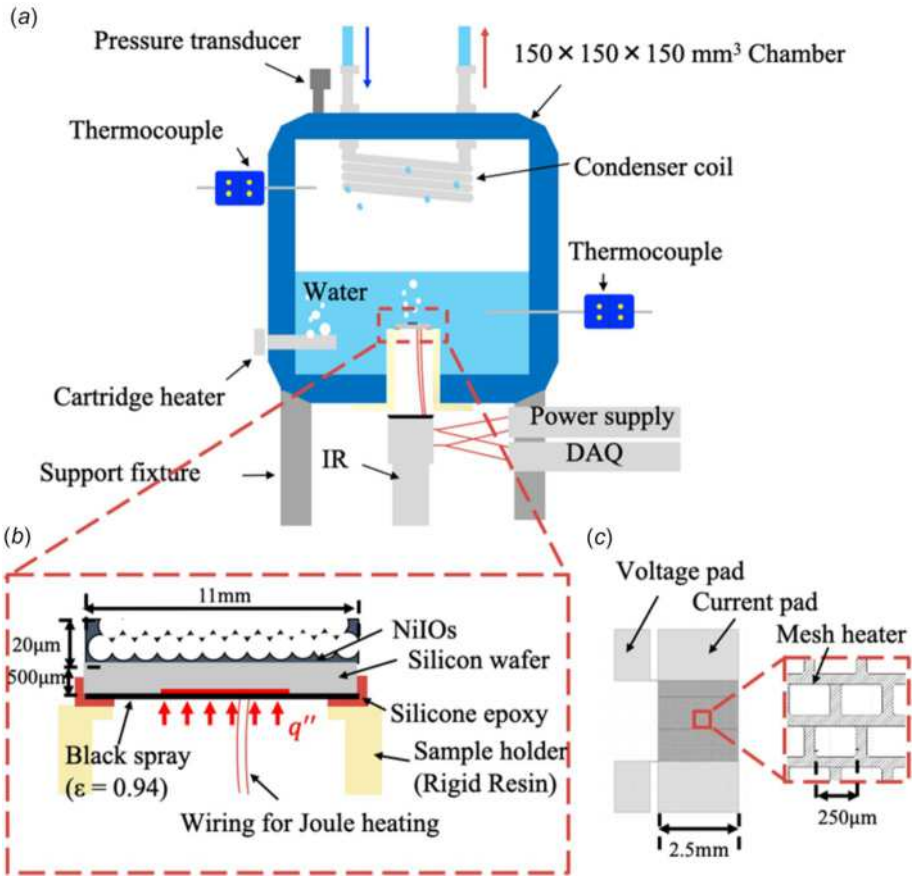

Fig. 2 (*a*) Pool boiling apparatus schematic, (*b*) zoomed-in view of NiIOs on sample holder, and (*c*) mesh heater, and the current and voltage pad patterned on the backside of the Si. Figure adapted from Ref. [8].

history of CuIOs and NiIOs during the 3-day reliability test still offered much insight into the thermal performance. For CuIOs, the temperature increased sharply between day 1 and day 2, indicating the start of thermal degradation. Throughout the 3 days, a temperature increase of over 14 °C was observed, equivalent to a decrease of heat transfer coefficient by half. However, for NiIOs, the temperature only marginally increased by 1.1 °C over the 3 days.

Imaging analysis for spatial temperature distribution and structural degradation of CuIOs and NiIOs samples is shown in Fig. 4. The IR images of the serpentine heater taken at 24-h intervals showed that hotspot appeared near the edge of the sample before day 2, and propagated inwards between day 2 and day 3. Cross-sectional SEM also confirmed that CuIOs structures, including spherical pore and neck features, were completely depleted after 3 days; only amorphous debris remained. This structural degradation was likely caused by corrosion-assisted erosion [7,8]. Corrosion, a strong function of temperature, happened uniformly on the surface of CuIOs and caused decrease in the mechanical strength of the inverse opal structures. Bubble formation and departure on surface, a strong function of heat flux, then physically eroded the inverse opal structures away.

Compared to CuIOs, NiIOs showed better resistance to such boiling-induced degradation. Ni is known for its corrosion resistance due to its protective oxide layer [9], chemical inertness, and high redox potential. Ni also has higher mechanical hardness compared to Cu as shown in Table 1, offering better erosion resistance. As shown in Fig. 4(*b*), no hotspot was observed on NiIOs sample throughout 3 days. The IO structures were also well preserved, with only the surface partially oxidized. It should be noted in Table 1 that Ni has a much lower thermal conductivity compared to Cu. However, due to the small μm-level thickness of the inverse opal structure, the resistance of the inverse opal layer was at least one order of magnitude lower than that of two-phase resistance in pool boiling. Therefore, the difference in thermal conductivity did not lead to a significant difference in thermal performance in this study.

Figure 5 shows the XPS results of the NiIOs sample before and after the reliability test. The sample surface was irradiated with X-rays, and the energies of the ejected photoelectrons were analyzed to determine surface composition. Three peaks at binding energy values of 529.7, 531.3, and 532.6 eV were detected on NiIOs before boiling. The 529.7 eV peak was NiO, a stable oxide formed in the presence of air. The 531.3 eV peak was likely nickel hydroxide, formed when NiIOs were immersed in water. We associated the 532.6 eV peak with surface contamination and impurities. After the 3-day reliability test, the shape and peak locations of electrons in the O1 s spectra (i.e., 1 s orbital of the oxygen atom) did not change much from that obtained earlier. The O1 s atomic ratio slightly increased from 30% to 35%, aligning with the oxidized surface observed in SEM. It should be noted that XPS is a highly surface-sensitive technique, and it can be susceptible to chemical contamination during cleaning and sample preparation (e.g., electrodeposition).

The results shown in this section indicate that NiIOs are a promising candidate for mitigating boiling-induced thermal degradation. However, as discussed earlier, there were variations in the thickness and neck-to-pore ratio across the tested sample. In addition, the effect of temperature on degradation cannot be ruled out; the initial T_{base} of CuIOs and NiIOs at the start of reliability test differed by over 5 °C. Section 3.2 covers a more controlled setup, where the heat flux was varied but the temperature was kept constant.

3.2 Effect of Heat Flux on Thermal Degradation. Figure 6(*a*) shows heat flux as a function of NiIOs base temperature, during pool

Downloaded from http://asmedigitalcollection.asme.org/electronicpackaging/article-pdf/147/4/041107/7524913/ep-25-1004.pdf by Stanford University user on 15 September 2025

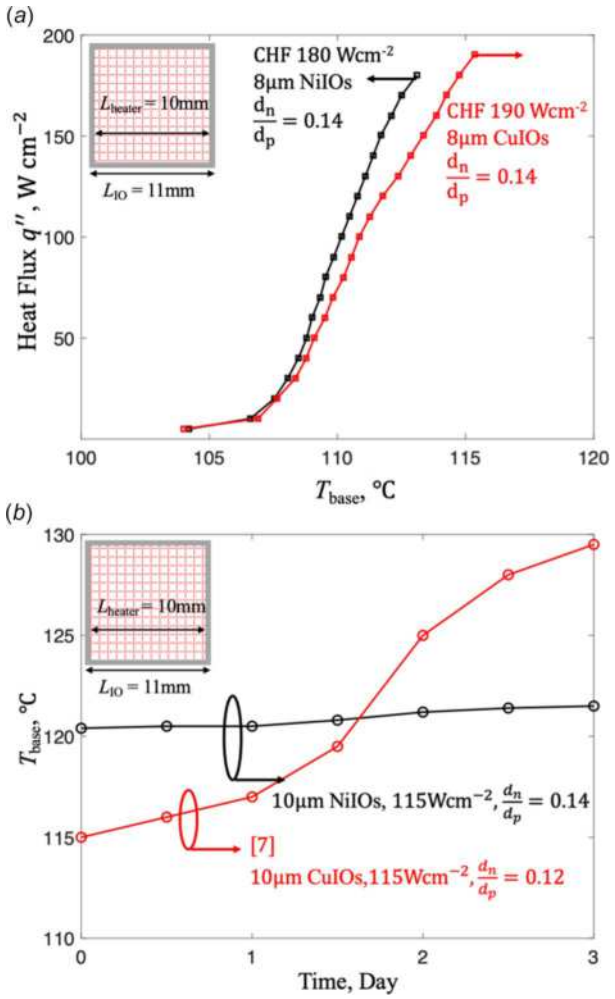

Fig. 3 (*a*) Average heat flux across the heated region as a function of CuIOs and NiIOs base temperature. CHF was measured to be 190 W cm^{-2} and 180 W cm^{-2}, for CuIOs and NiIOs, respectively. Both samples reported are of IO thickness 8 μm, neck-to-pore ratio 0.14, pore diameter 4.8 μm, IO-covered area 11 × 11 mm^2, and heated area 10 × 10 mm^2. (*b*) Time history of CuIOs (red curve) and NiIOs (black curve) base temperature over 3-day pool boiling reliability test, at a constant heat flux of 115 W cm^{-2}. CuIOs sample is of thickness 10 μm, neck-to-pore ratio 0.12, and NiIOs sample is of thickness 10 μm, neck-to-pore ratio 0.14. The initial T_{base} is different from that reported in (*a*) at q'' = 115 W cm^{-2}, likely due to the difference in thickness and neck-to-pore ratio.

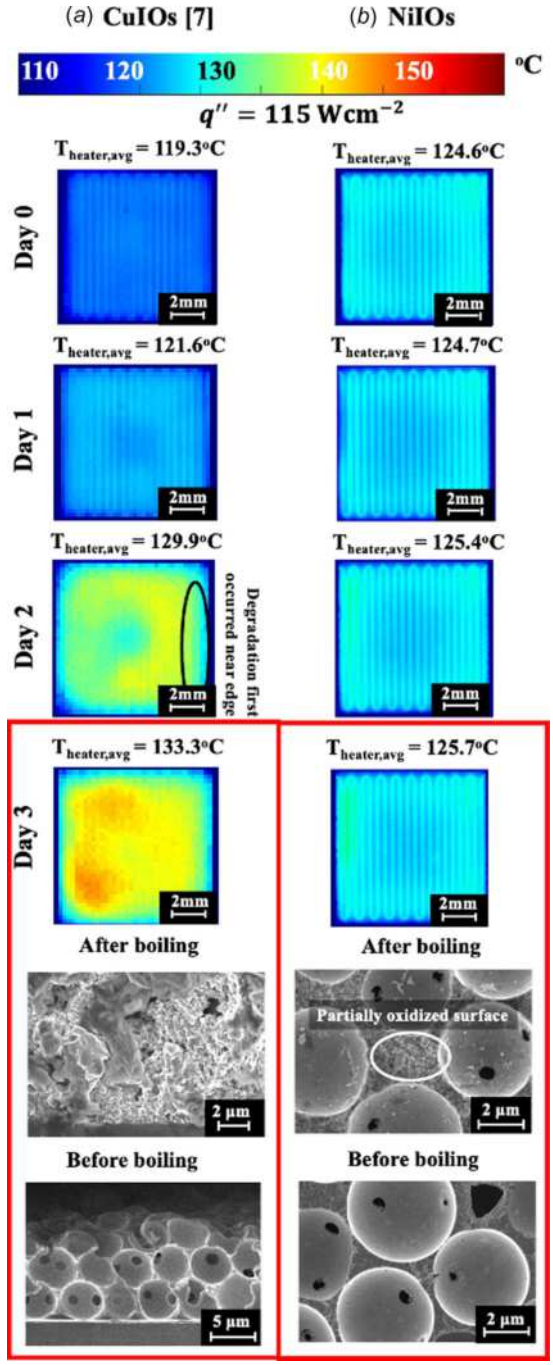

Fig. 4 Infrared image of heater at 24-h interval throughout 3-day reliability test, conducted at constant q'' = 115 W cm^{-2}. SEM of IO structures before and after boiling reliability test. (*a*) CuIOs of 10-μm thickness, neck-to-pore ratio of 0.12 and (*b*) NiIOs of 10-μm thickness, neck-to-pore ratio of 0.14.

boiling test at 1.01×10^5 Pa. The NiIOs were of thickness 20 μm, neck-to-pore ratio 0.14, and coverage area of 11 × 11 mm^2. The CHF of 375 W cm^{-2} was achieved using a heater size of 2.5 × 2.5 mm^2. The CHF of this sample was much higher than that reported in Fig. 3, due to the smaller bubble size and the heater size matching the characteristic length of the water bubbles [8]. Notably, the pool boiling curve had a very sharp slope, and the superheat was only 7.2 °C at the CHF. The dashed line in Fig. 6(*a*) represents the three tested heat fluxes 75 W cm^{-2}, 150 W cm^{-2}, and 225 W cm^{-2} during the reliability test, where the superheat difference between these three heat fluxes was within 0.5 °C.

Nickel inverse opals of the same dimension as that in the CHF test were used for the reliability test over 3 days, and the recorded temperature history is shown in Fig. 6(*b*). The heat flux was supplied with a 2.5 × 2.5 mm^2 mesh heater at q'' = 0 (heater off), 75 W cm^{-2} (20% CHF), 150 W cm^{-2} (40% CHF), and 225 W cm^{-2} (60% CHF). By increasing the applied heat flux, the bubble size did not increase significantly, due to water bubble characteristic length (~2.7 mm)

Table 1 Nickel and copper material property comparison

Description	Ni	Cu
Density, g cm^{-3}	8.88	8.96
Ultimate tensile strength, MPa	317	210
Young's modulus, GPa	207	140
Vickers hardness, MPa	638	369
Thermal conductivity, W m^{-1} K^{-1}	60.7	398

Downloaded from http://asmedigitalcollection.asme.org/electronicpackaging/article-pdf/147/4/041107/7524913/ep-25-1004.pdf by Stanford University user on 15 September 2025

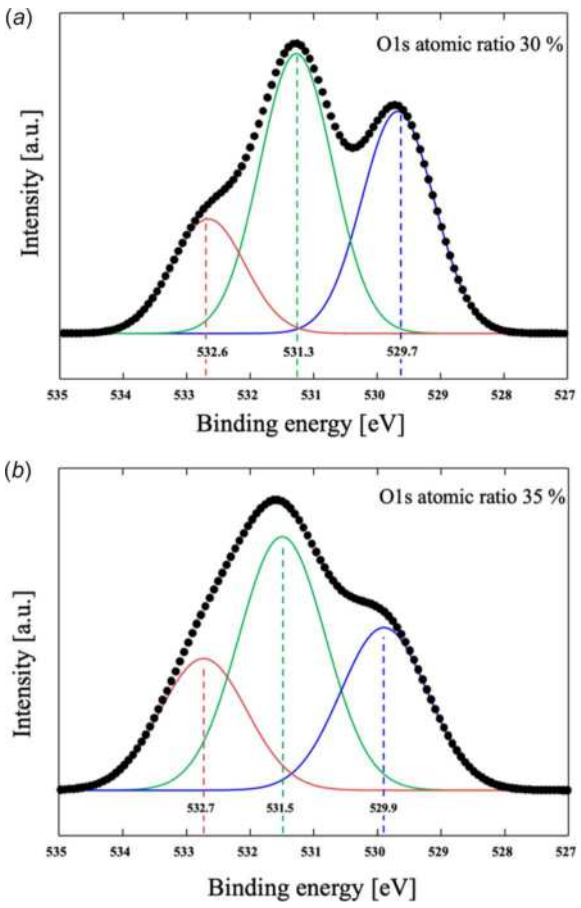

Fig. 5 High-resolution O1 s spectra of NiIOs surface (*a*) before and (*b*) after 3-day reliability test. Spectra was obtained using XPS.

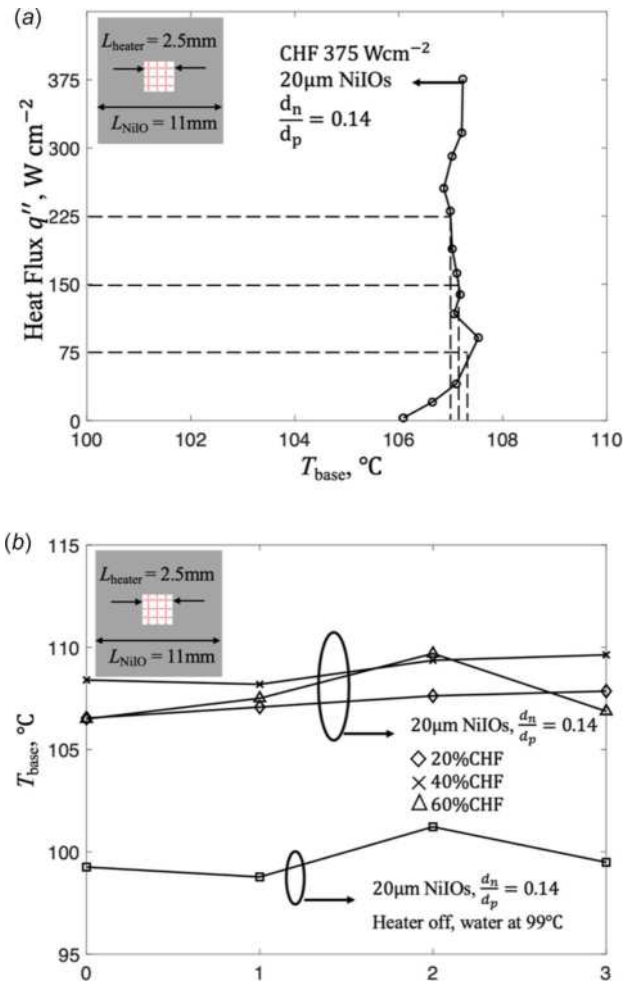

Fig. 6 (*a*) Average heat flux across the heated region as a function of NiIOs base temperature. CHF was measured to be 375 W cm^{-2}. NiIOs sample has a thickness of 20 μm, neck-to-pore ratio of 0.14, pore diameter 4.8 μm, IO-covered area of 11 × 11 mm^2, and heated area of 2.5 × 2.5 mm^2. At various supplied heat fluxes (e.g., 75 W cm^{-2}, 150 W cm^{-2}, and 225 W cm^{-2} as shown in the dotted line), the temperature of the NiIOs base did not vary by more than 0.5 °C. (*b*) Time history of NiIOs base temperature over 3-day pool boiling reliability test, at a heat flux of 75 W cm^{-2} (20% CHF), 150 W cm^{-2} (40% CHF), 225 W cm^{-2} (60% CHF), and 0 W cm^{-2} (heater off). NiIOs sample has a thickness of 20 μm, and neck-to-pore ratio of 0.14.

matching the heater size (2.5 mm). However, the bubble formation and departure frequency increased with increasing heat flux [12–14]. The effect of temperature could be excluded here because the IO base temperature varies little heat flux, as shown in Fig. 6(*a*).

The time history of NiIOs at various heat fluxes increased marginally, by 1.2 °C to 3.2 °C, across 3 days, indicating minimum decrease in the heat transfer coefficient. In addition, no hot spot was observed in the IR images shown in Fig. 7. The SEM images were taken at two locations: the center of the heated region (i.e., active boiling region) and the edge (i.e., nondirectly heated region, no bubble formation or departure). In the cross-sectional SEM view, no full-layer depletion of NiIOs was observed in any of the three samples. However, the top view SEM offered more insights. The 20% and 40% CHF samples showed only partially oxidized surfaces in both the heated and nondirectly heated regions, similar to that seen in Fig. 4. No structural degradation was observed. However, the 60% CHF sample, with the highest bubble formation and departure rate, showed depletion of the top-half spheres at the center heated region. The degradation was the most severe at the center of the heater due to the highest erosion rate during active boiling. We also observed that degradation happened on the top layer first, where bubble formation, departure, and coalescence took place, and propagated gradually downwards. Future work should focus on imaging of bubble dynamics at the top surface to better understand the erosion mechanism.

4 Conclusions

In conclusion, this study investigated the potential of NiIOs in mitigating thermal degradation induced by boiling, particularly in comparison to CuIOs. Through pool boiling tests conducted over three days, it was observed that NiIOs exhibited significantly less thermal degradation compared to CuIOs, attributed to the inherent corrosion resistance and mechanical strength of nickel. SEM only showed partial oxidation on the NiIOs surface, and the IO structures were preserved. Surface analysis using XPS showed an increased level of oxidation after boiling, aligning with the SEM findings. More controlled tests were done to analyze the effect of heat flux degradation. For heat flux levels of 20% to 40% CHF, NiIOs showed minimal degradation. However, for a heat flux of 60% CHF, NiIOs experienced high bubble formation and departure frequency, causing the top half layer to be eroded away. These findings underscore the potential of NiIOs as a promising solution for long-term thermal management in high-power electronic devices. However, to ensure long lifetime of such porous media, design considerations should be made for operation within an allowable maximum heat flux range. Further research should focus on bubble imaging and analysis to better understand the erosion process. Also, reliability tests of NiIOs under various operating conditions should be done for integration into real-world applications.

Downloaded from http://asmedigitalcollection.asme.org/electronicpackaging/article-pdf/147/4/041107/7524913/ep-25-1004.pdf by Stanford University user on 15 September 2025

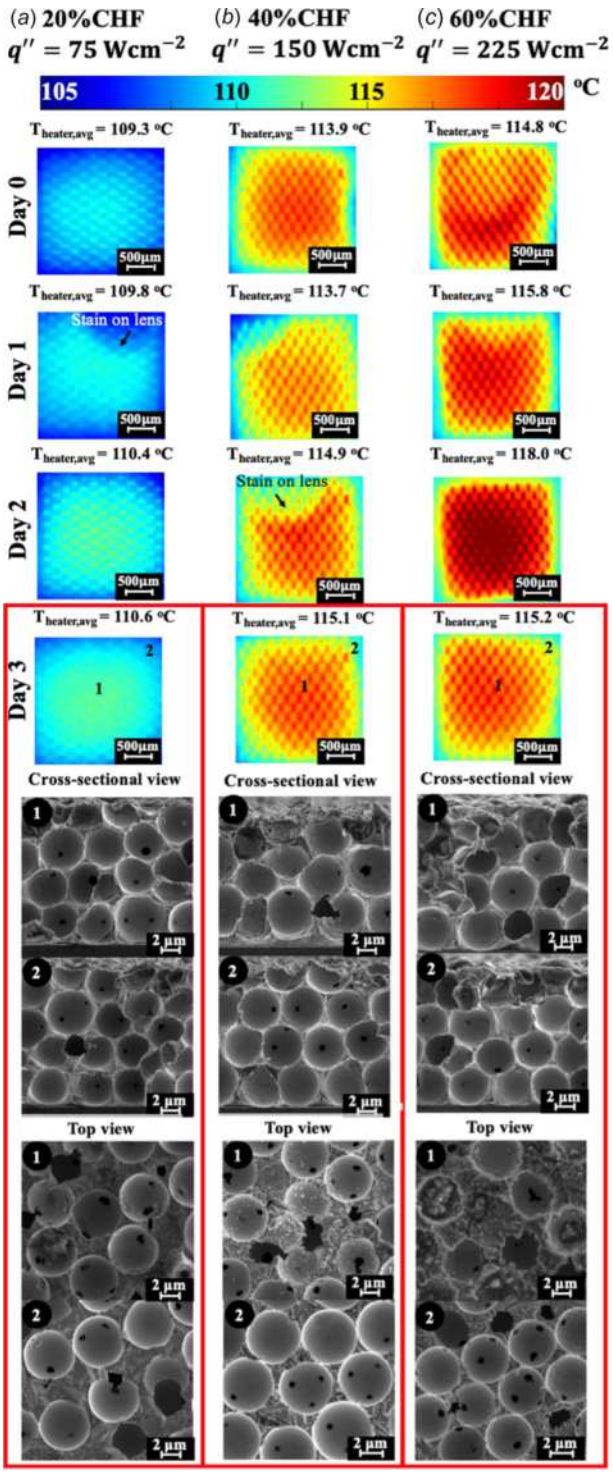

Fig. 7 Infrared image of the heater at 24 h interval throughout 3-day reliability test at various heat fluxes: (*a*) $q'' = 75$ W cm^{-2}, (*b*) 150 W cm^{-2}, and (*c*) 225 W cm^{-2}. Cross-sectional SEM images at center (i.e., directly heated region) and edge of the heater (i.e., nondirectly heated region) were taken after 3 days. Tested samples were all NilOs of 20-μm thickness.

Acknowledgment

We acknowledge the financial support from the Advanced Research Projects Agency-Energy (ARPA-E) under the Agreement No. DE-FOA-0001858, "Exploring the limits of cooling for extreme heat flux applications: data centers and power electronics." Part of this work was performed at the Stanford Nanofabrication Facility (SNF) and Stanford Nanofabrication Shared Facilities (SNSF), supported by the National Science Foundation under Award No. ECCS-2026822.

This work was co-authored by the National Renewable Energy Laboratory (NREL), operated by Alliance for Sustainable Energy, LLC, for the U.S. Department of Energy (DOE) under Contract No. DE-AC36-08GO28308. Funding was provided by ARPA-E. The views expressed in the article do not necessarily represent the views of the DOE or the U.S. Government.

This work was supported by the Korea Institute of Energy Technology Evaluation and Planning (KETEP) grant funded by the Ministry of Trade, Industry & Energy, Korea (Grant No. 20212020800270).

Funding Data

- Advanced Research Projects Agency-Energy (ARPA-E) (Agreement No. DE-FOA-0001858; Funder ID: 10.13039/100006133).
- National Science Foundation (Award No. ECCS-2026822; Funder ID: 10.13039/100000001).
- National Renewable Energy Laboratory (NREL), operated by Alliance for Sustainable Energy, LLC, for the U.S. Department of Energy (DOE) (Contract No. DE-AC36-08GO28308; Funder ID: 10.13039/100006233).
- Korea Institute of Energy Technology Evaluation and Planning (KETEP) grant funded by the Ministry of Trade, Industry & Energy, Korea (Grant No. 20212020800270; Funder ID: 10.13039/501100007053).

Conflict of Interest

There is no conflict of interest.

Data Availability Statement

The datasets generated and supporting the findings of this article are obtainable from the corresponding author upon reasonable request.

Nomenclature

d = diameter of the pore or the neck (μm)
j = current density (mA cm^{-2})
k = thermal conductivity (W cm^{-1} K^{-1})
L = length of the square heater or the IO coverage region (mm)
q'' = heat flux (W cm^{-2})
t = thickness of the substrate (m)
T = temperature (°C)
ε = emissivity

Subscripts

avg = average value
base = base of the porous IO, on the top side of the Si substrate
Cu = copper
heater = patterned mesh heater, on the bottom side of the Si substrate
IO = porous inverse opal
n = neck of the IO, controlled by sintering temperature and time
Ni = nickel
p = pore of the IO, controlled by the diameter of polystyrene beads
Si = silicon substrate

References

[1] Fang, J., Li, H., Tang, Y., and Blaabjerg, F., 2019, "On the Inertia of Future More-Electronics Power Systems," IEEE J. Emerging Sel. Top. Power Electron., **7**(4), pp. 2130–2146.

Downloaded from http://asmedigitalcollection.asme.org/electronicpackaging/article-pdf/147/4/041107/7524913/ep-25-1004.pdf by Stanford University user on 15 September 2025

[2] Khan, N., Pinjala, D., and Toh, K. C., 2004, "Pool Boiling Heat Transfer Enhancement by Surface Modification/Micro-Structures for Electronics Cooling: A Review," Proceedings of the Sixth Electronic Packaging Technology Conference (EPTC), Singapore, Dec. 8–10, pp. 273–280.
[3] Jaikumar, A., and Kandlikar, S. G., 2015, "Enhanced Pool Boiling Heat Transfer Mechanisms for Selectively Sintered Open Microchannels," Int. J. Heat Mass Transfer, **88**, pp. 652–661.
[4] Ha, M., and Graham, S., 2019, "Pool Boiling Enhancement Using Vapor Channels in Microporous Surfaces," Int. J. Heat Mass Transfer, **143**, p. 118532.
[5] Zhang, C., Rong, G., Palko, J. W., Dusseault, T. J., Asheghi, M., Santiago, J. G., and Goodson, K. E., 2015, "Tailoring of Permeability in Copper Inverse Opal for Electronic Cooling Applications," ASME Paper No. IPACK2015-48262.
[6] Won, Y., Barako, M. T., Agonafer, D. D., Asheghi, M., and Goodson, K. E., 2014, "Mechanical and Thermal Properties of Copper Inverse Opals for Two-Phase Convection Enhancement," Proceedings of the 14th Intersociety Conference on Thermal and Thermomechanical Phenomena in Electronic Systems (ITherm), Orlando, FL, May 27–30, pp. 326–332.
[7] Kong, D., Kim, K., Jung, E., Jiang, K., Wu, Q., Jang, B., Kwon, H., Asheghi, M., Goodson, K. E., and Lee, H., 2024, "Boiling-Induced Thermal Degradation of Copper Inverse Opals and Its Mitigation," Int. Commun. Heat Mass Transfer, **151**, p. 107250.
[8] Jiang, K., Kong, D., Kim, K., Narumanchi, S., Palko, J. W., Dede, E. M., Ahn, C., Lee, H., Asheghi, M., and Goodson, K. E., 2024, "Pool Boiling Reliability Tests and Degradation Mechanisms of Microporous Copper Inverse Opal (CuIOs) Structures," Proceedings of the 23rd Intersociety Conference on Thermal and Thermomechanical Phenomena in Electronic Systems (ITherm), Aurora, CO, May 28–31, pp. 1–8.
[9] Muhamed Shajudheen, V. P., Anitha Rani, K., Senthil Kumar, V., Uma Maheswari, A., Sivakumar, M., and Saravana Kumar, S., 2018, "Comparison of Anticorrosion Studies of Titanium Dioxide and Nickel Oxide Thin Films Fabricated by Spray Coating Technique," Mater. Today: Proc., **5**(2), pp. 8889–8898.
[10] Huang, Y. S., Zeng, X. T., Hu, X. F., and Liu, F. M., 2004, "Corrosion Resistance Properties of Electroless Nickel Composite Coatings," Electrochim. Acta, **49**(25), pp. 4313–4319.
[11] Rao, S., and Balakrishnan, A., 1997, "Analysis of Pool Boiling Heat Transfer Over Porous Surfaces," Heat Mass Transfer, **32**(6), pp. 463–469.
[12] Ivey, H. J., 1967, "Relationships Between Bubble Frequency, Departure Diameter and Rise Velocity in Nucleate Boiling," Int. J. Heat Mass Transfer, **10**(8), pp. 1023–1040.
[13] Hamzekhani, S., Falahieh, M. M., Kamalizadeh, M. R., and Nazari, Z., 2015, "Experimental Study on Bubble Departure Frequency for Pool Boiling of Water/NaCl Solutions," Heat Mass Transfer, **51**(9), pp. 1313–1320.
[14] Chen, C. A., Li, K. W., Lin, T. F., Li, W. K., and Yan, W. M., 2021, "Study on Heat Transfer and Bubble Behavior Inside Horizontal Annuli: Experimental Comparison of R-134a, R-407C, and R-410A Subcooled Flow Boiling," Case Stud. Therm. Eng., **24**, p. 100875.

Downloaded from http://asmedigitalcollection.asme.org/electronicpackaging/article-pdf/147/4/041107/7524913/ep-25-1004.pdf by Stanford University user on 15 September 2025